Hindawi
Evidence-Based Complementary and Alternative Medicine
Volume 2019, Article ID 8128170, 16 pages
https://doi.org/10.1155/2019/8128170

Research Article

Uncovering the Anticancer Mechanism of Compound Sophorae Decoction against Ulcerative Colitis-Related Colorectal Cancer in Mice

Shuangjiao Deng,[1] Qing Tang,[1] Xueyun Duan,[2,3] Heng Fan,[1] Lijuan Zhang,[1] Xiwen Zhu,[1] Jianli Hu,[4] Meng Xu,[1] Qianyun Chen,[1] Yujin Liu,[1] Yalan Dong,[1] Zhen Nan,[5] and Hui Wu[1]

[1]*Department of Integrated Traditional Chinese and Western Medicine, Union Hospital, Tongji Medical College, Huazhong University of Science and Technology, Wuhan 430022, China*
[2]*Department of Pharmacy, Hubei Provincial Hospital of Traditional Chinese Medicine, Wuhan 430061, China*
[3]*Department of Pharmacy, Hubei Province Academy of Traditional Chinese Medicine, Wuhan 430074, China*
[4]*Cancer Center, Union Hospital, Tongji Medical College, Huazhong University of Science and Technology, Wuhan 430022, China*
[5]*Department of Geriatrics, Hubei Xinhua Hospital, Wuhan 430015, China*

Correspondence should be addressed to Heng Fan; fanheng009@aliyun.com and Lijuan Zhang; 614365168@qq.com

Received 30 May 2019; Accepted 4 August 2019; Published 20 October 2019

Academic Editor: Barbara Romano

Compound sophorae decoction (CSD), a traditional Chinese medicine (TCM) formula, has been voluminously used in China to deal with ulcerative colitis and gained significant therapeutic effect. Tremendous explorations have unraveled a contributory role of inflammatory bowel disease (IBD) like ulcerative colitis (UC) and Crohn's disease (CD) at the onset of colorectal cancer, scilicet, and colitis-related cancer (CRC). In light of the anti-inflammatory properties of CSD in UC, we appraised its chemoprevention capacity and underlying mechanism in ulcerative colitis-related colorectal cancer (UCRCC), employing a model of azoxymethane (AOM) plus dextran sulfate sodium- (DSS-) induced colorectal cancer (CRC) in C57BL/6 mice. Rapturously, our results illuminated the ameliorative effect of CSD against UCRCC in mice portrayed by lesser polyps or adenomas, attenuated colonic xenograft tumor growth in company with the preferable well-being of mice in contrast to the Model Group. We examined significant downregulation of proinflammatory cytokines such as TNF-α, NF-κB, IL-6, STAT3, and IL-17 after exposure to CSD, with the concomitant repression of inflammation-associated proteins, including COX-2 and iNOS. Independent of this, treatment with CSD declined the proportion of T helper 17 cells (Th17) and protein level of matrix metallopeptidase 9 (MMP-9). Moreover, transmission electron microscopy (TEM) detected observably suppressed mitophagy in mice administered with CSD and that was paralleled by the pro-apoptotic effect as indicated by upregulating caspase-3 together with caspase-9 and deregulating B-cell lymphoma 2 (Bcl-2). In closing, these findings suggest CSD executes the UCRCC-inhibitory activity through counteracting inflammatory responses and rescuing detuning of apoptosis as well as neutralizing overactive mitophagy, concurring to build up an oncosuppressive microenvironment.

1. Introduction

Ulcerative colitis (UC) is a long-lasting and relapsing inflammatory intestinal disturbance, whose etiology and pathogenesis is still elusive, with a growing body of compelling evidence defining its promoting role in the initiation of colorectal cancer [1–3]. It has been well-acknowledged that long-standing proinflammatory cytokines comprising tumor necrosis factor (TNF-α), interleukin- (IL-) 17, and NF-κB/IL-6/STAT3 cascade in colon harbor a close relationship between UC and colon cancer and simultaneously behave as pivotal mediators in the onset and deterioration of UC and colorectal cancer [4–9]. Accordingly, these data underscore a crucial role of proinflammatory responses in

the context of UCRCC and confer the urgency to address the related concrete mechanism.

Mitochondria are cardinal double membrane-bound organelles and cellular stress sensors involved in multifaceted cellular activities containing energy production, senescence, apoptosis, oxidative stress regulation, and metabolism in addition to signaling. Hence, these cellular properties of mitochondria denote a highly-associated link connecting cellular dysfunction in the context of cancer or noncancer and abnormalities in mitochondrial status along with activity and meanwhile, authenticate the magnitude of the timely elimination of damaged and aged mitochondria which is called mitophagy for maintaining the cellular integrity [10–17]. To our knowledge, cancer is a disturbance in the homeostatic balance between cell growth and cell death, which is featured by metabolic reprogramming, uncontrolled cellular proliferation, and enhanced resistance to apoptosis of tumor cell. Massive reports [10–12, 16, 17] have identified that mitophagy is activated under conditions of stimuli such as nutrient depletion, hypoxia, and activated oncogenes, imparting considerable flexibility for tumor cell growth and survival. In addition, mitochondria-targeted drugs and targeting apoptosis pathways open up the opportunity for the development of novel therapeutic strategies for cancer abrogation [10, 11]. Therefore, it is anticipated that a broad understanding of mitophagy and apoptosis in UCRCC may shed light on investigating the tumor-promoting mechanisms to the next level.

Compound sophorae decoction (CSD) is a classical traditional Chinese medicine (TCM) preparation developed from qingre zaoshi liangxue fang (QRZSLXF) [18] has been widely applied in China to medicate UC patients and is clinically efficient [19, 20]. Kushen, videlicet, *Sophora flavescens* Ait., is the sovereign drug of CSD and is used extensively to treat fibrosis, asthma, inflammatory disorders, ulcers, and solid tumor [19–26]. However, definitive mechanisms that demonstrate the role of CSD in UCRCC are still obscure. Thereby, further studies analyzing the contribution of CSD to the amelioration of UCRCC and identifying its active ingredients via mass spectrometry (MS) appear warranted.

Taken together, we hypothesize that inflammatory responses along with uncontrollable homeostasis between mitophagy and cellular apoptosis synergistically facilitate the formation of ambience in favor of UCRCC, and CSD overturns the tumourigenesis effect (Figure 1(a)). This study may provide novel insights into the carcinogenesis of UCRCC and open a promising therapeutic approach to UCRCC.

2. Materials and Methods

2.1. Animals and Mouse Model of UCRCC. Male C57BL/6J mice (6–8 weeks old) were lodged under specific pathogen-free (SPF) conditions with free access to autoclaved food and water in the experimental animal center of Huazhong University of Science and Technology (HUST, Wuhan, China). They were stochastically grouped into Model Group (AOM/DSS), CSD Group (AOM/DSS + CSD), and Normal Group. UCRCC model was conducted based on a typical protocol [27, 28], that is, the administration of a single intraperitoneal injection of AOM (12 mg/kg, Sigma) in conjunction with three rounds of 2.5% DSS (36–50 kDa; MP Biochemicals) application (Figure 1(b)). All animal care and experimental processes were performed in accordance with guidelines of the Animal Research Institute Committee of HUST and National Institutes of Health guidelines and regulations.

2.2. Composition and Preparation of CSD. CSD is a Chinese herbal mixture composed of *Sophora flavescens* Ait. (15 gram), Radix Sanguisorbae (15 gram), Indigo Naturalis (3 gram), *Bletilla striata* (Thund.) Reichb. f. (10 gram), *Panax notoginseng* (Burk.) F. H. Chen (3 gram), and *Glycyrrhiza uralensis* Fisch. (10 gram). All the raw herbal medicines were purchased from Hubei Provincial Hospital of Traditional Chinese Medicine (Wuhan, China) and then mixed according to the weight ratio before soaking for 1 h. Eventually, the mixture was condensed into a concentration of 1.076 g/ml as CSD and stored at 4°C after undergoing initial hard boil and being simmered for 1 h and incurring succedent filter. 150 μl CSD was administrated by gavage daily, synchronizing the procedure of DSS induction.

2.3. Behavioral and Physiological Assessment. Body weight, stool consistency, and hemafecia ratio in addition to intake of food and water were recorded daily throughout the whole span of the experiment. After figuring out weight and length of colons, the number and diameter of tumors were calculated.

2.4. Western Blot Analysis. Proteins of each colon were extracted in RIPA buffer supplemented with phosphatase and protease inhibitors. 40 μg proteins were utilized for the investigation of inflammatory responses in the colon as described previously [29]. Antibodies recognizing the proteins were as follows: anti-IL-6 (1 : 500, Bioss, Beijing, China), anti- TNF-α (1 : 1000, Abcam, Cambridge, UK), anti-NF-κB (1 : 2000, Cell Signaling Technology, USA), and anti-IL-17 (1 : 1000, Abcam, Cambridge, UK).

2.5. Histological Evaluation and Immunohistochemistry. Fresh colon sections were embedded in paraffin after being fixed in 4% paraformaldehyde and then were cut into 4 μm slides that would be stained with haematoxylin-eosin (H&E) hereafter. An expert pathologist carried out histopathological examinations blindly. For immunohistochemical assessment, the paraffin-embedded colonic slides were subjected to immunohistochemical staining and incubated with primary antibodies for cyclooxygenase-2 (COX-2; 1 : 100, Cell Signaling Technology, USA), inducible nitric oxide synthase (iNOS; 1 : 100, Boster, Wuhan, China), matrix metallopeptidase 9 (MMP-9; 1 : 100, Ruiying Biological, Suzhou, China), TNF-α (1 : 50, Santa, Dallas, TX, USA), B-cell lymphoma 2 (Bcl-21 : 100, Boster, Wuhan, China), caspase-3 (1 : 100; PTG, Wuhan, China), and caspase-9

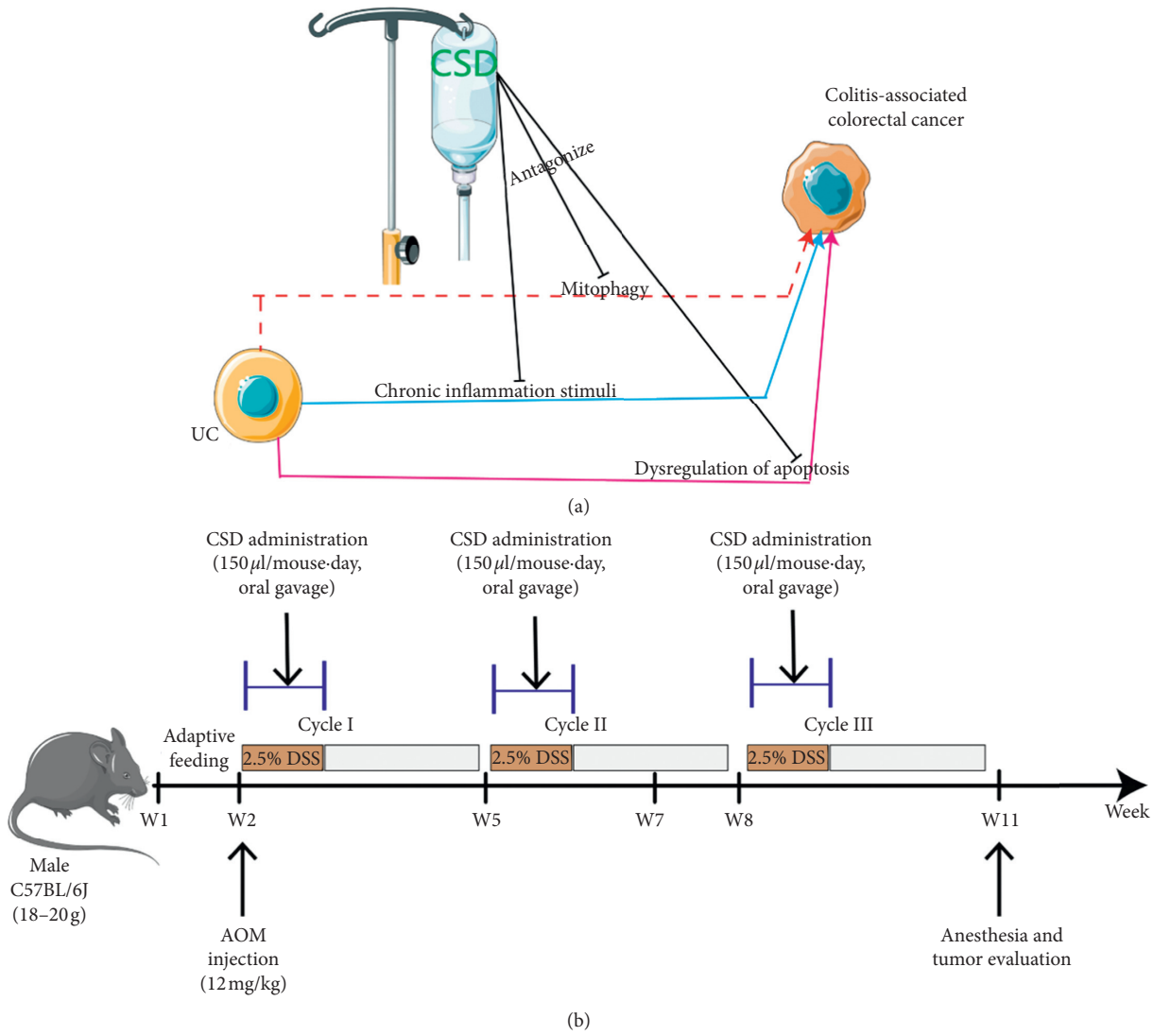

Figure 1: A schematic diagram of the workflow of CSD in UCRCC (a) and experimental protocol for UCRCC model and validation for investigation of the mechanisms of CSD (b).

(1 : 100; Boster, Wuhan, China) complying with the manufactures' protocols.

2.6. Transmission Electron Microscopy Observation. For the transmission electron microscopic (TEM) analysis of mitochondria, pretreated colon tissues underwent a series of procedures reported as previously [10] and the stained ultrathin colonic sections (60–80 nm) were detected using a Hitachi-HT7700 electron microscope (Tokyo, Japan).

2.7. Flow Cytometry. After being stimulated with phorbol myristate acetate (PMA; Abcam, Cambridge, UK), ionomycin, and GolgiPlug protein transport inhibition (BD Biosciences, San Diego, USA) in a humidified 37°C and 5% CO_2 incubator for 7 h, single-cell suspension of splenocytes and mesenteric lymph nodes (MLNs) were stained with FITC-labeled antimouse CD4 and PE-labeled antimouse IL-17A antibodies (BD Biosciences, MD, USA). Isotype antibody was adopted as the negative control. Thenceforward, the stained cells were washed and analyzed by using a FACSCalibur flow cytometer (BD Biosciences, San Diego, CA).

2.8. High-Resolution Metabolomics. 100 μl CSD liquid samples underwent methanol extraction by adding 900 μl methanol or pure water extraction by adding 900 μl pure water, following the procedures listed as follows: vortexing for 1 min; centrifuging for 10 min, 12000 r/min, 4°C; filtering the supernatant through a 2 μm filter; and analyzing the filtrate on the machine. Untargeted metabolic profiling of CSD was performed employing high-resolution mass spectrometry (HRMS; Q-Exactive High-Resolution Mass Spectrometer, Thermo Fisher Scientific). Analyte separation was accomplished with the aid of liquid chromatography (UltiMate 3000 RS, Thermo Fisher Scientific) fitted with chromatographic column (Thermo Hypersil GOLD 100 × 2.1 mm,

1.9 μm) manoeuvred at 0.3 mL/min with aqueous phase (0.1% aqueous formic acid) and organic phase (0.1% formic acid acetonitrile). The operating gradient came as follows: 0–2 min (aqueous phase: 95% ⟶ 80%, organic phase: 5% ⟶ 20%); 2–6 min (aqueous phase: 80% ⟶ 25%, organic phase: 20% ⟶ 75%); 6–8.5 min (aqueous phase: 25% ⟶ 5%, organic phase: 75% ⟶ 95%); 8.5–12.5 min (aqueous phase: 5%, organic phase: 95%); 12.5–13 min (aqueous phase: 5% ⟶ 95%, organic phase: 95% ⟶ 5%); and 13–16 min (aqueous phase: 95%, organic phase: 5%).

The electrospray ionization source was performed in positive ion mode with a spray voltage of 3.8 kV, capillary temperature of 300°C, sheath gas (nitrogen, purity ≥99.999%) flow of 40 arbitrary units (Arb), and auxiliary gas (nitrogen, purity ≥99.999%) temperature of 350°C. The resolution was set to 70000 (full mass), 17500 (dd-MS2), and the scan range was 70–1000 m/z. Data acquisition time was 16 min.

Mass spectral features represented by accurate mass m/z, retention time, and intensity were detected by high-resolution FTMS and sorted using CD2.1 software (Thermo Fisher) and then identified, aligned, and quantified according to databases such as Mzcloud, MzVault, and ChemSpider with the value of mzCloud Best Match ≥80%.

2.9. Statistical Analysis. All experimental data obtained from this study were presented as mean ± standard deviation (SD). Statistical significance between the data from different groups was calculated by one-way analysis of variance (ANOVA) or Student's t-test using SPSS software (version 19.0). A p value <0.05 was deemed as statistically significant.

3. Results

3.1. CSD Upgrades Clinical Symptoms in Mice Treated with AOM/DSS and Allays AOM/DSS-Induced Malignancy. As shown in Figure 2(a), significant body weight loss during the experimental period in mice from Model Group compared with Normal Group was alleviated by CSD administration, particularly after the third DSS cycle. In agreement with this, CSD treatment posed a decrement in the incidence ratio of hematochezia accompanied by postponed occurrence of diarrhea and blood in feces, as evaluated (Figure 2(b)). The shortening of colons, signifying the aggravation of colonic damage, was observed in mice exposed to AOM/DSS in comparison with mice in the CSD Group ($p < 0.05$) (Figures 2(c) and 2(d)). Furthermore, our data manifested higher polyp/adenoma multiplicity escorted by higher grade of epithelial dysplasia in the Model Group (Figures 2(e) and 2(f)).

3.2. CSD Moderates the Malignant Inflammatory Features in AOM/DSS-Induced UCRCC. Incremental expression of proinflammatory cytokines such as NF-κB and TNF-α and overactivation of IL-6/STAT3 passage have been well determined to exercise definitive implication in the pathogenesis of UC and colon cancer. In line with this, mice received AOM/DSS exhibited a rise in intestinal production of these parameters and IL-17 concentration in comparison with Normal Group, whereas intake of CSD significantly reversed the reaction expectably as illustrated by western blot and immunohistochemistry (Figures 3(a)–3(c)). Given the traditional role of Th17 cells in binding UC and UCRCC together, we explored the disparities in the proportion of Th17 cells isolated from spleens and MLNs of mice via flow cytometry (Figure 3(d)). Not surprisingly, the analysis revealed that Th17 cells may prompt the incipience of UCRCC and can be partially overthrown by CSD (Figure 3(e)). Regarding intestinal iNOS and COX-2 expression profiles, they were incremental in colon tissues from mice treated with AOM/DSS compared with the untreated mice, being diminished by treatment with CSD (Figure 3(f)).

3.3. CSD Modulates Ultrastructural Changes and Apoptosis in AOM/DSS-Induced Mice. Apoptosis and mitophagy are two representative procedures that act in synergy to regulate cell survival and death in numerous types of cancer. To gain further insight into the pattern of CSD on apoptosis and mitophagy, we determined the changes in the levels of apoptosis regulatory proteins and mitochondrial morphology in the colons with the aid of immunohistochemical staining and TEM, respectively. The data came out with significant up-regulation of mitochondrial cleaved-caspase-3, caspase-9 and down-regulation of Bcl-2 in colons after implementing CSD therapy, evincing the apoptosis-encouraging efficacy of CSD (Figure 4(a)). We extended our attempts to probe mitochondrial structure from TEM images (Figure 4(b)), as demonstrated by the phenomenon that there was a pronounced increase in vacuolization (black asterisk panels), massive mitochondrial fission and loss of cristae as well as highly electron-condensation (arrowheads), and even lysosomes engulfing damaged mitochondria (arrows) in Model Group. To the contrary, the conspicuous mitochondrial morphological alternations brought on by AOM/DSS were perceptibly absent following CSD administration (Figure 4(b)), establishing mitophagy as an etiological factor in UCRCC tumorigenesis. The expression profile of MMP-9, whose well-appreciated pathologies is the relationship to cancer owing to its role in extracellular matrix remodeling and angiogenesis, was depicted to experience a slight diminution inflicted by CSD (Figure 3(f)).

3.4. Identification of Chemical Ingredients in CSD by Mass Spectrographic Analysis. We attempted to identify the active constituents in CSD using high-resolution mass spectrometry (HRMS) and part of a summary of the various abundant constituents detected and identified by the channel of methanol extraction (Figure 5(a)) and pure water extraction (Figure 5(b)) was given, respectively. HRMS confirmed oxymatrine as the most abundant ingredient in the CSD liquid (Figures 5(a) and 5(b)). The active compounds from CSD extraction through methanol extraction were as follows: oxymatrine, isoliquiritigenin, (−)-maackiain, DL-stachydrine, cytisine, indirubin, 18-β-glycyrrhetinic acid, ginsenoside Rg3, licochalcone A,

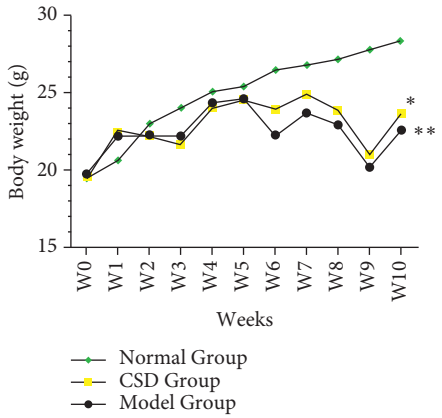

(a)

(c)

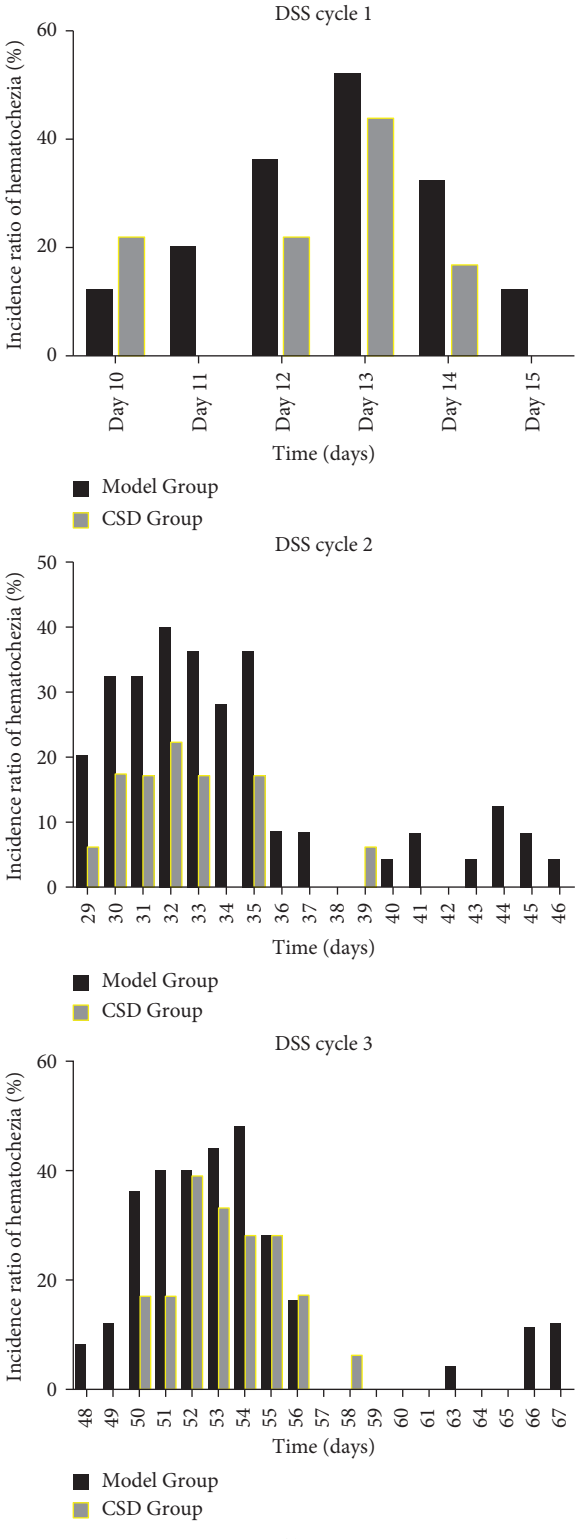

(b)

Figure 2: Continued.

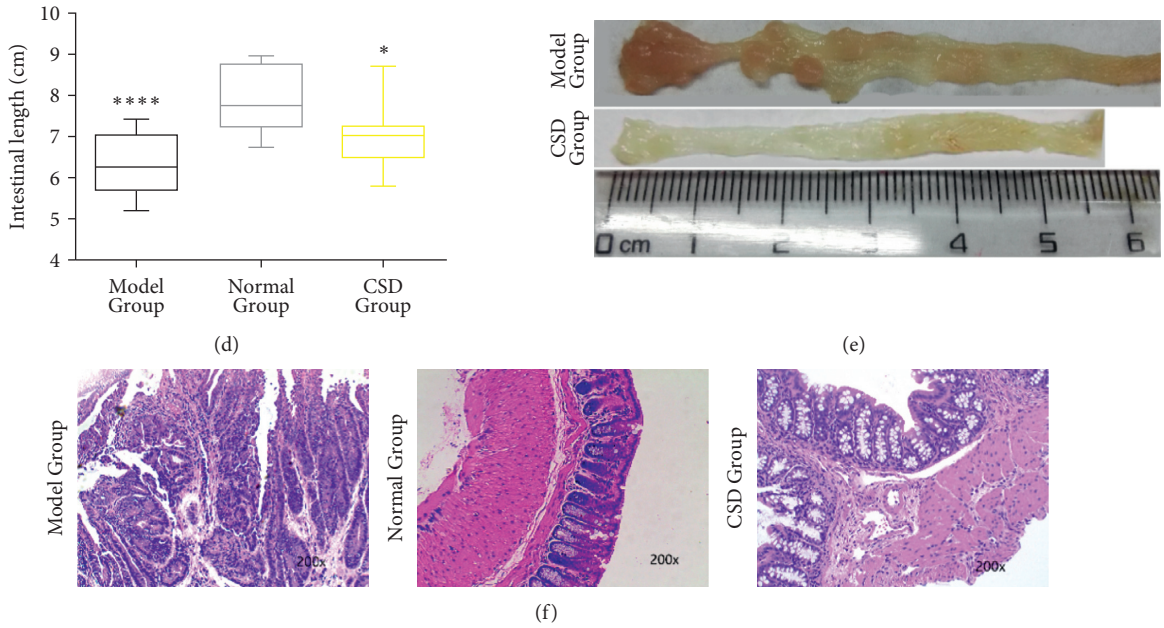

Figure 2: CSD overcomes AOM/DSS-induced malignancy of colon. (a) Body weight per mouse measured per day during all the experiment. $^{*}p < 0.05$, $^{**}p < 0.01$, significantly different from the Normal Group. (b) Effect of CSD on the incidence ratio of hematochezia. $^{*}p < 0.05$ vs. Model Group. (c) Colonic length of mice from the three groups. (d) Comparison of colon length among the three groups, $^{*}p < 0.05$, $^{**}p < 0.01$ vs. Normal Group. (e) Effect of CSD on multiplicity of polyp/adenoma on colons. (f) Colon sections stained with H&E (×200) from each group.

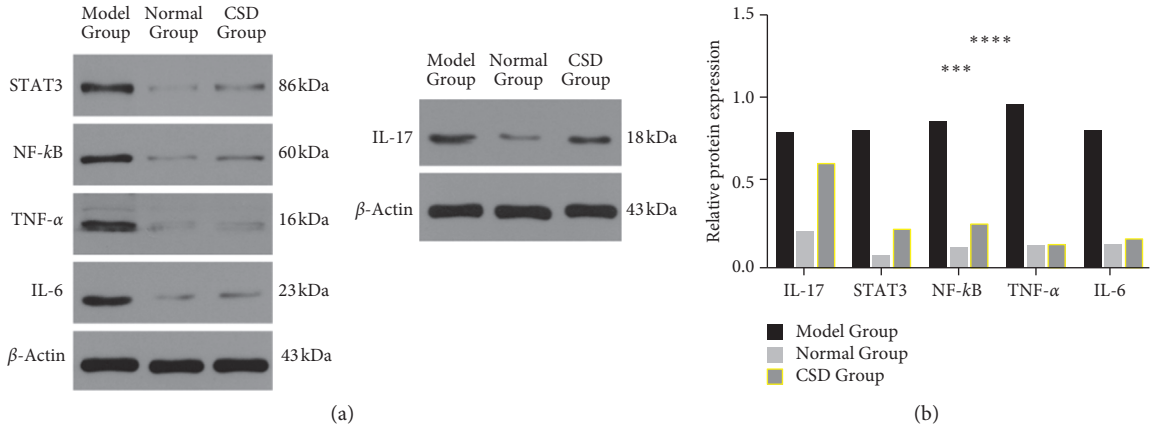

Figure 3: Continued.

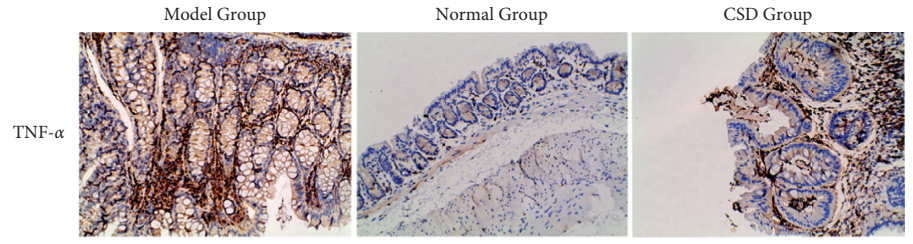

(c)

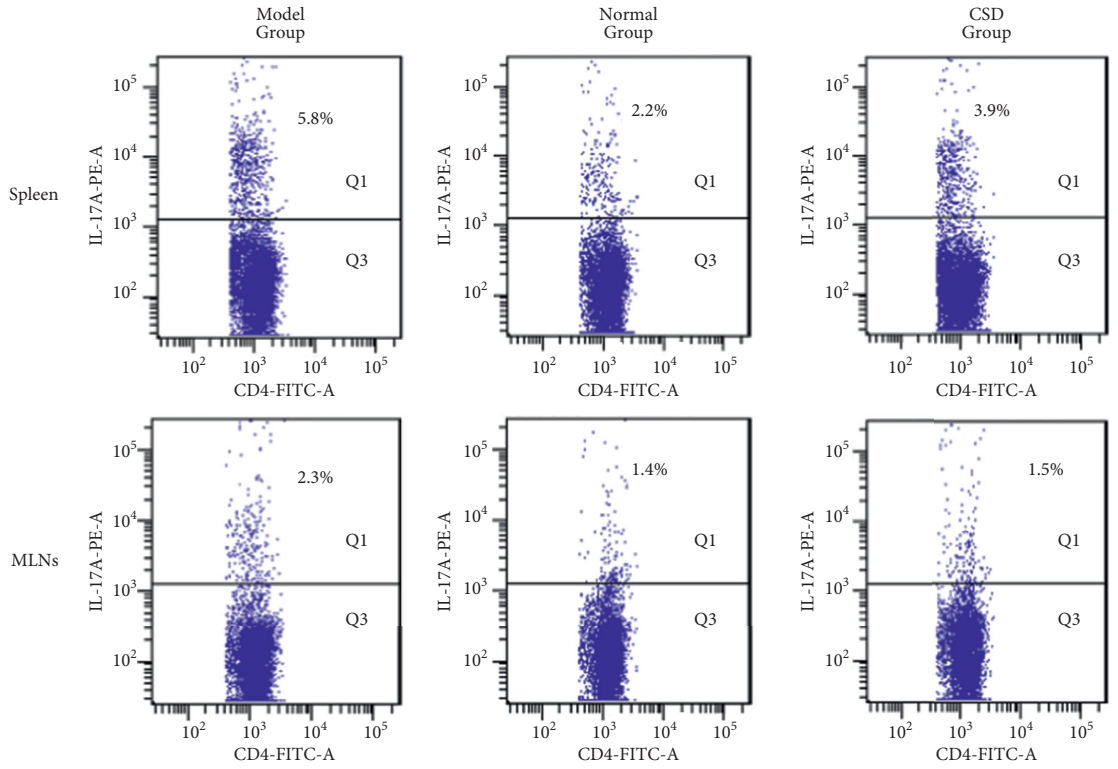

(d)

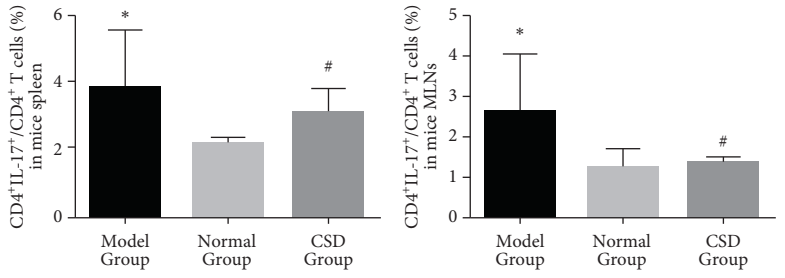

(e)

Figure 3: Continued.

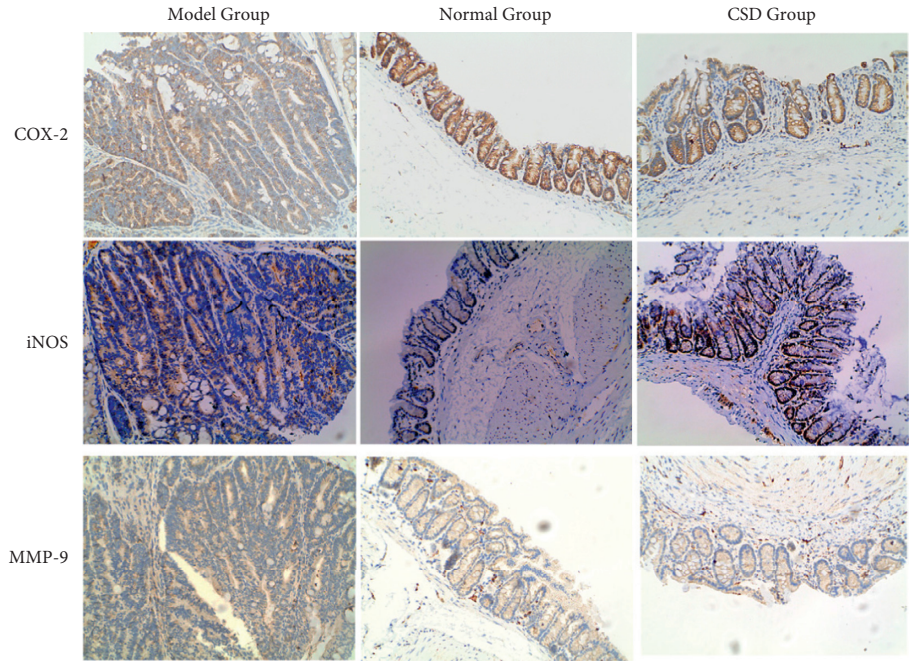

(f)

Figure 3: AOM/DSS-induced inflammatory response is impeded by CSD. (a) Western blot analysis of classical inflammatory proteins expression profiles in colon. (b) Representative histogram of densitometry analysis of the data derived from western blot, $^{**}p < 0.01$, significantly different from the Model Group. (c) Immunohistochemical staining analysis of TNF-α expression in colons. (d) Representative flow cytometry dot plot of the percentages of $CD4^{+}IL\text{-}17^{+}$Th17 cells in CD4+ cells in the spleen and MLNs of each group. (e) Trends of Th17 cells in mice, $^{*}p < 0.05$, $^{\#}p > 0.05$ vs. Model Group. (f) Effect of CSD on COX-2, iNOS, and MMP-9 expression in colon tissues in C57BL/6 mice.

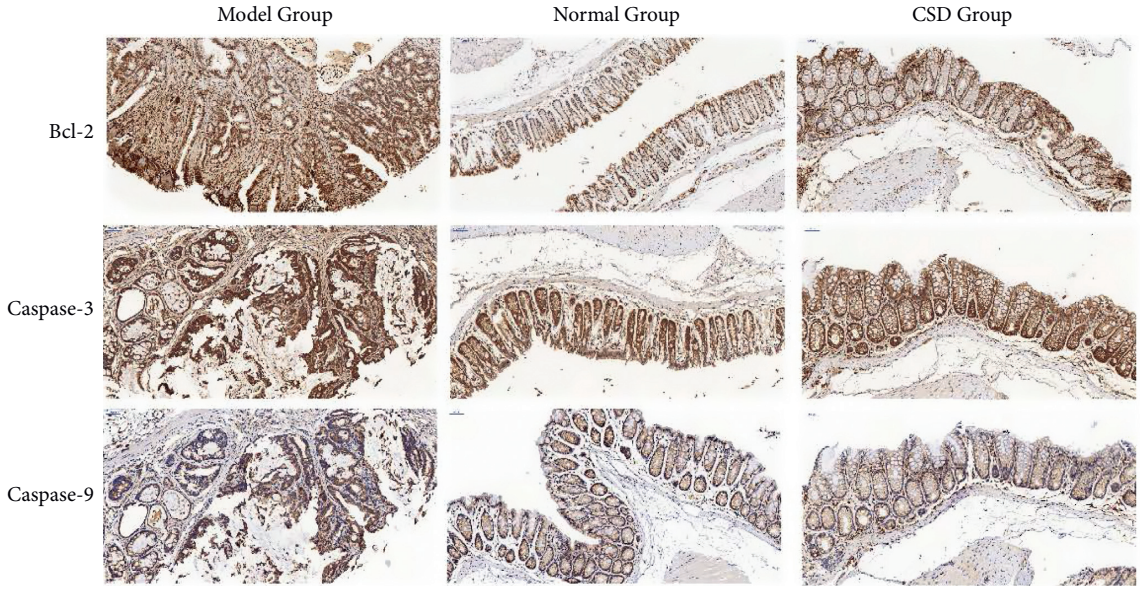

(a)

Figure 4: Continued.

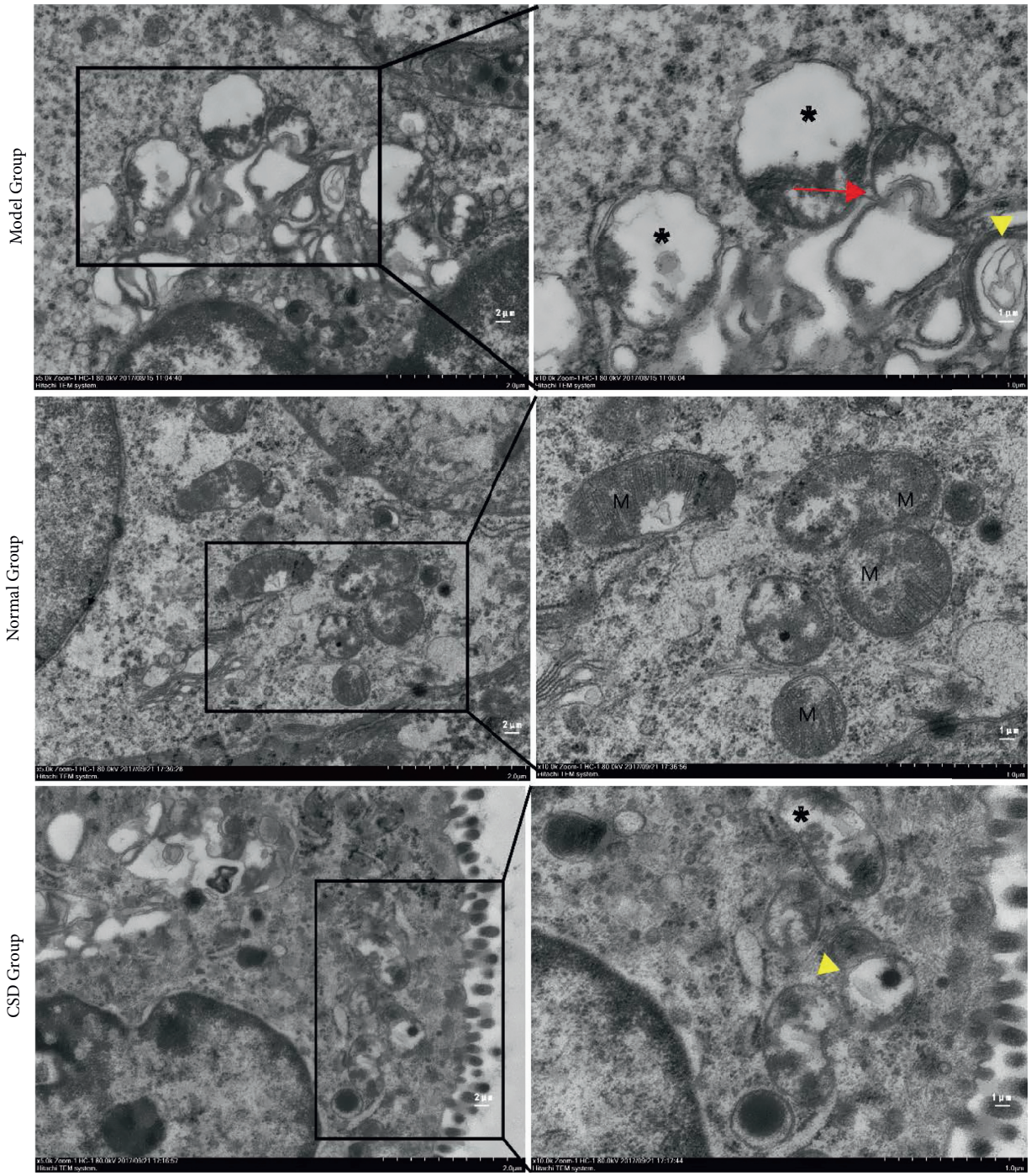

(b)

Figure 4: (a) CSD attunes apoptosis-related proteins expression language illustrated by immunohistochemistry. (b) Electron micrographs of mitochondrial morphology colonic tissues in mice. Arrowheads indicate the disrupted mitochondria undergoing mitochondrial fission, absence of cristae or electron-condensation; Arrows symbolize lysosomes engulfing damaged mitochondria. M means mitochondrion.

Name	Formula	Annotation Source: Predicted Compositions	Annotation Source: mzCloud Search	Annotation Source: ChemSpider Search	Annotation Source: MassList Match	FISh Coverage	Molecular Weight	RT [min]	Area (Max.)	# ChemSpider Results	# mzCloud Results	# mzVault Results	mzCloud Best Match	Group Area: F2
Oxymatrine	C15 H24 N2 O2	Full match	Full match	Partial match	Full match	16.07	264.1833	2.316	515109927	2	6	0	95.7	515109927.3
Proline	C5 H9 N O2	Full match	Full match	Full match	Full match	-	115.0635	0.961	131425796	50	4	0	85.8	131425795.9
Dibutyl phthalate	C16 H22 O4	Full match	Full match	Full match	Full match	-	278.1515	8.352	48424764.8	21	9	0	95.2	48424764.81
Isoliquiritigenin	C15 H12 O4	Full match	Full match	Full match	Full match	54.55	256.0731	4.506	48376399.4	34	6	0	97.3	48376399.37
DL-Arginine	C6 H14 N4 O2	Full match	Full match	Full match	Full match	-	174.1116	0.799	44987026.2	7	4	0	93.2	44987026.15
Bis(4-ethylbenzylidene)sorbitol	C24 H30 O6	Full match	Full match	Partial match	Full match	-	414.2037	7.155	40586940.1	8	4	0	94.9	40586940.07
Hexamethylenetetramine	C6 H12 N4	Full match	Full match	Full match	No results	17.65	140.106	14.473	38328386.8	3	2	0	97.4	38328386.75
Erucamide	C22 H43 N O	No match	Invalid mass	No match	No results	45.07	320.3071	11.739	35366872.9	1	2	0	95.7	35366872.87
D-(+)-Maltose	C12 H22 O11	No match	Invalid mass	No match	No results	-	364.0978	0.944	28665838.1	2	4	0	89.8	28665838.11
Choline	C5 H13 N O	Full match	Full match	Partial match	Full match	-	103.1001	0.808	25933085.1	12	2	0	85.2	25933085.13
(-)-Maackiain	C16 H12 O5	Full match	Full match	Partial match	Full match	-	284.0681	5.404	24623436.9	42	16	0	88.5	24623436.89
Asparagine	C4 H8 N2 O3	Full match	Full match	Partial match	Full match	-	132.0536	0.966	21140114.9	27	6	0	86.8	21140114.93
L-Norleucine	C6 H13 N O2	Full match	Full match	Not the top hit	Full match	-	131.0947	1.35	19032179.1	56	10	0	86	19032179.1
DL-Stachydrine	C7 H13 N O2	Full match	Full match	Partial match	Full match	-	143.0946	0.933	12954247.6	52	2	0	86.2	12954247.61
Trigonelline	C7 H7 N O2	Full match	Full match	Not the top hit	Full match	-	137.0476	0.982	12927754.5	47	18	0	91.8	12927754.52
Cytisine	C11 H14 N2 O	Full match	Full match	Not the top hit	Full match	-	190.1106	0.876	12783681.3	32	2	0	89.6	12783681.35
L-Phenylalanine	C9 H11 N O2	Full match	Full match	Full match	Full match	34.78	165.079	1.931	11606902	95	4	0	95.4	11606902.02
DL-Tryptophan	C11 H12 N2 O2	No match	Invalid mass	No match	No match	63.04	187.0636	3.067	11467917.6	33	6	0	96.9	11467917.59
5-Hydroxymethyl-2-furaldehyde	C6 H6 O3	Full match	Full match	Partial match	Full match	-	126.0318	1.946	10120207	26	18	0	88.2	10120207.04
Formononetin	C16 H12 O4	Full match	Full match	Full match	Full match	47.17	268.0732	6.188	7676456.6	34	4	0	96.5	7676456.596
3-Hydroxy-2-methylpyridine	C6 H7 N O	Full match	Full match	Not the top hit	Full match	-	109.0531	0.907	7058284.23	36	15	0	86.4	7058284.229
α-Lactose	C12 H22 O11	No match	Invalid mass	No match	No results	-	359.1424	1.343	6851306.67	2	2	0	87.8	6851306.672
Maltol	C6 H6 O3	Full match	Full match	Partial match	Full match	-	126.0318	2.749	6495269.32	26	12	0	88.4	6495269.32
Ononin	C22 H22 O9	Full match	Full match	Not the top hit	Full match	-	430.1261	5.161	6324440.85	5	2	0	91	6324440.854
Oleamide	C18 H35 N O	No match	Invalid mass	No match	No results	36.51	264.2451	9.847	5130179.81	5	2	0	97.2	5130179.81
Indirubin	C16 H10 N2 O2	Full match	Full match	Full match	No results	-	262.0739	6.761	5005072.7	9	10	0	90	5005072.7
Stearamide	C18 H37 N O	Full match	Full match	Full match	Full match	-	283.287	10.645	4477466.55	4	3	0	94.2	4477466.549
Anthranilic acid	C7 H7 N O2	Full match	Full match	Partial match	Full match	-	137.0476	4.242	4072977.66	47	18	0	92.7	4072977.662
Betulin	C30 H50 O2	Full match	Full match	Partial match	Full match	-	442.3806	5.596	3488495.57	42	2	0	83.5	3488495.572
18-β-Glycyrrhetinic acid	C30 H46 O4	Full match	Full match	Partial match	Full match	14.91	470.3392	6.089	3457136.7	23	2	0	96.9	3457136.704

Name	Formula	Annotation Source: Predicted Compositions	Annotation Source: mzCloud Search	Annotation Source: ChemSpider Search	Annotation Source: MassList Match	FISh Coverage	Molecular Weight	RT [min]	Area (Max.)	# ChemSpider Results	# mzCloud Results	# mzVault Results	mzCloud Best Match	Group Area: F2
18-β-Glycyrrhetinic acid	C30 H46 O4	Full match	Full match	Partial match	Full match	14.91	470.3392	6.089	3457136.7	23	2	0	96.9	3457136.704
α-Eleostearic acid	C18 H30 O2	Full match	Full match	Partial match	Full match	-	278.2245	7.936	3189018.09	19	3	0	92.2	3189018.093
(3S,4R)-3-(1-hydroxyhexyl)-4-(	C11 H20 O4	No match	Invalid mass	No match	No results	-	198.1255	6.84	3184569.78	4	2	0	83.8	3184569.784
L-Histidine	C6 H9 N3 O2	Full match	Full match	Full match	Full match	-	155.0695	0.828	3131520.41	18	3	0	90.1	3131520.407
Hexadecanamide	C16 H33 N O	Full match	Full match	Full match	Full match	-	255.256	9.729	3032768.98	4	2	0	91.9	3032768.978
3-[2-(3-Hydroxyphenyl)ethyl]-5	C15 H16 O3	Full match	Full match	Partial match	No results	-	244.1097	6.2	2567369.03	36	6	0	92.3	2567369.032
Bis(2-ethylhexyl) phthalate	C24 H38 O4	Not the top hit	Full match	Full match	Full match	-	390.2761	11.144	2420907.38	26	10	0	94	2420907.381
2-Hydroxyphenylalanine	C9 H11 N O3	No match	Invalid mass	No match	No match	-	164.0475	1.195	2309984.25	41	5	0	88.1	2309984.246
Adenosine	C10 H13 N5 O4	Full match	Full match	Not the top hit	Full match	-	267.0965	0.88	2270151.36	34	1	0	80.9	2270151.362
9-Oxo-10(E),12(E)-octadecadi	C18 H30 O3	Full match	Full match	Not the top hit	Full match	-	294.2194	8.157	2180416.19	24	2	0	95	2180416.19
Glycitin	C22 H22 O10	Not the top hit	Full match	Partial match	Full match	-	446.1211	4.432	2099593.48	11	2	0	87.7	2099593.479
Ginsenoside Rg3	C42 H72 O13	No match	Invalid mass	No match	No results	-	766.4856	5.594	2096363.33	1	4	0	82.7	2096363.325
D-(-)-Glutamine	C5 H10 N2 O3	Full match	Full match	Full match	Full match	-	146.0691	0.948	1867381	31	6	0	84.6	1867381
Docosanamide	C22 H45 N O	Full match	Full match	No results	Full match	-	339.3495	13.084	1574239.28	0	2	0	93.2	1574239.278
Licochalcone A	C21 H22 O4	Full match	Full match	Partial match	No results	-	338.1515	6.997	1571849.91	15	4	0	89.8	1571849.911
PEG n10	C20 H42 O11	Not the top hit	Full match	Full match	Full match	-	458.2729	4.159	1477574.46	1	2	0	87.9	1477574.46
Xantholumol	C21 H22 O5	Full match	Full match	Full match	Full match	-	354.1463	6.238	1448182.69	25	8	0	90.8	1448182.689
7,8-Dihydroxy-4-methylcoumar	C10 H8 O4	Full match	Full match	Not the top hit	Full match	-	192.0425	3.723	1432077.92	38	8	0	87.9	1432077.925
Daidzein	C15 H10 O4	Full match	Full match	Full match	Full match	-	254.0577	5.231	1268752.83	44	4	0	90.6	1268752.828
PEG n5	C10 H22 O6	Full match	Full match	Full match	Full match	-	238.1418	2.86	1146294.07	1	4	0	81.2	1146294.075
N,N'-Dicyclohexylurea	C13 H24 N2 O	Full match	Full match	Full match	Full match	-	224.1887	6.574	1070298.03	6	2	0	93	1070298.034
PEG n11	C22 H46 O12	Not the top hit	Full match	No results	Full match	-	502.299	4.283	1053909.78	0	2	0	87	1053909.777
Naringenin	C15 H12 O5	Full match	Full match	Full match	Full match	-	272.0683	4.447	975615.82	46	10	0	88.1	975615.82
2-Hydroxyphenylalanine	C9 H11 N O3	No match	Invalid mass	No match	No match	-	164.0475	0.886	857402.572	41	3	0	80.3	857402.5722
Sakuranetin	C16 H14 O5	Full match	Full match	Full match	Full match	-	286.0841	5.263	789959.076	44	7	0	80.7	789959.0762
1-Linoleoyl glycerol	C21 H38 O4	Full match	Full match	Partial match	No results	-	354.2766	9.33	773589.134	5	2	0	92.8	773589.1341
Leucylproline	C11 H20 N2 O3	Full match	Full match	Partial match	Full match	-	228.1475	2.99	734846.835	6	4	0	81.5	734846.8345
Guanine	C5 H5 N5 O	Full match	Full match	Partial match	Full match	-	151.0494	1.188	676845.058	20	1	0	80.6	676845.0576
Monobutyl phthalate	C12 H14 O4	Full match	Full match	Partial match	Full match	-	222.089	6.331	613928.87	45	4	0	85	613928.8697
3,4-Dihydroxyphenylpropionic a	C9 H10 O4	No match	Invalid mass	No match	No match	-	164.0475	3.368	558873.06	41	3	0	84.1	558873.0596

(a)

Figure 5: Continued.

Name	Formula	Annotation Source: Predicted Compositions	Annotation Source: mzCloud Search	Annotation Source: ChemSpider Search	Annotation Source: MassList Match	FISh Coverage	Molecular Weight	RT [min]	Area (Max.)	# ChemSpider	# mzCloud Results	# mzVault Results	mzCloud Best Match	Group Area: F8
Oxymatrine	C15 H24 N2 O2	Full match	Full match	Partial match	Full match	14.55	264.18303	2.356	579229024.8	2	6	0	95.7	579229025
Proline	C5 H9 N O2	Full match	Full match	Full match	Full match	-	115.06352	0.865	128291737.3	50	4	0	83.2	128291737
Dibutyl phthalate	C16 H22 O4	Full match	Full match	Full match	Full match	47.83	278.15139	8.357	43509917.34	21	6	0	95.1	43509917.3
Isoliquiritigenin	C15 H12 O4	Full match	Full match	Full match	Full match	45.1	256.0732	4.513	43149066.46	34	6	0	97.5	43149066.5
Hexamethylenetetrami	C6 H12 N4	Full match	Full match	Full match	No results	23.53	140.10596	14.469	36810028.01	3	2	0	97.5	36810028
L-Pyroglutamic acid	C5 H7 N O3	Full match	Full match	Not the top hit	Full match	-	129.04274	1.145	31014849.17	24	4	0	81.7	31014849.2
Choline	C5 H13 N O	Full match	Full match	Partial match	Full match	-	103.10012	0.816	28680713.24	12	2	0	82.6	28680713.2
DL-Stachydrine	C7 H13 N O2	Full match	Full match	Partial match	Full match	-	143.09467	1.062	23521925.51	52	4	0	85.2	23521925.5
DL-Arginine	C6 H14 N4 O2	No match	Invalid mass	No match	No results	-	157.08506	0.82	22767400.18	5	2	0	93.5	22767400.2
L-Norleucine	C6 H13 N O2	Full match	Full match	Not the top hit	Full match	-	131.09474	1.357	21421231.76	56	10	0	89	21421231.8
Pipecolic acid	C6 H11 N O2	Full match	Full match	Not the top hit	Full match	-	129.0791	0.955	20770655.33	68	8	0	82.8	20770655.3
Cytisine	C11 H14 N2 O	Full match	Full match	Not the top hit	Full match	33.33	190.11061	1.096	20174721.62	32	4	0	95.6	20174721.6
Asparagine	C4 H8 N2 O3	No match	Invalid mass	No match	No match	-	115.02698	0.844	17236595.01	11	4	0	86.4	17236595
D-(+)-Maltose	C12 H22 O11	No match	Invalid mass	No match	No results	-	364.0978	0.828	16746970.51	2	4	0	90.9	16746970.5
Trigonelline	C7 H7 N O2	Full match	Full match	Not the top hit	Full match	-	137.04758	0.867	14037685.87	47	18	0	93.7	14037685.9
(+)-Maackiain	C16 H12 O5	Full match	Full match	Partial match	Full match	-	284.06816	5.404	13303900.11	42	24	0	93.4	13303900.1
L-Phenylalanine	C9 H11 N O2	No match	Invalid mass	No match	No match	39.13	148.05249	1.985	12962993.12	33	4	0	96.9	12962993.1
DL-Tryptophan	C11 H12 N2 O2	No match	Invalid mass	No match	No match	-	187.06349	3.094	10793994.04	33	6	0	94.9	10793994
3-Hydroxy-2-methylpy	C6 H7 N O	Full match	Full match	Not the top hit	Full match	-	109.05311	0.862	8755620.954	36	10	0	86.5	8755620.95
Ononin	C22 H22 O9	Not the top hit	Full match	Not the top hit	Full match	-	430.12602	5.17	6128388.745	5	2	0	90.1	6128388.74
L-Tyrosine	C9 H11 N O3	No match	Invalid mass	No match	No match	-	164.04753	1.166	5143034.87	41	6	0	85.8	5143034.87
5-Hydroxymethyl-2-fu	C6 H6 O3	Full match	Full match	Partial match	Full match	-	126.03195	2.037	4956561.398	26	12	0	89.1	4956561.4
Erucamide	C22 H43 N O	Full match	Full match	Partial match	Full match	39.13	337.33367	11.764	4661529.045	3	3	0	95.9	4661529.04
18-β-Glycyrrhetinic ac	C30 H46 O4	Not the top hit	Full match	Partial match	Full match	15.88	470.3391	6.089	4402208.806	23	2	0	96.7	4402208.81
Anthranilic acid	C7 H7 N O2	Full match	Full match	Partial match	Full match	-	137.04758	4.271	3986402.448	47	12	0	93.5	3986402.45
α-Lactose	C12 H22 O11	Full match	Full match	Not the top hit	Full match	-	342.11555	5.593	3745394.204	17	2	0	86.9	3745394.2
Adenosine	C10 H13 N5 O4	Full match	Full match	Not the top hit	Full match	-	267.0967	1.069	3565462.707	34	2	0	89.8	3565462.71
L-Glutamine	C5 H10 N2 O3	No match	Invalid mass	No match	No match	-	129.04262	0.842	3447711.429	24	3	0	86.3	3447711.43
(3S,4R)-3-(1-hydroxyl	C11 H20 O4	No match	Invalid mass	No match	No results	-	198.12547	6.861	3107090.822	4	3	0	83.7	3107090.82
Betulin	C30 H50 O2	Full match	Full match	Partial match	Full match	-	442.38046	5.59	2850840.167	42	2	0	83.7	2850840.17

Name	Formula	Annotation Source: Predicted Compositions	Annotation Source: mzCloud Search	Annotation Source: ChemSpider Search	Annotation Source: MassList Match	FISh Coverage	Molecular Weight	RT [min]	Area (Max.)	# ChemSpider	# mzCloud Results	# mzVault Results	mzCloud Best Match	Group Area: F8
Betulin	C30 H50 O2	Full match	Full match	Partial match	Full match	-	442.38046	5.59	2850840.167	42	2	0	83.7	2850840.17
PEG n10	C20 H42 O11	Not the top hit	Full match	Full match	Full match	-	458.27269	4.161	2782623.267	1	2	0	88.1	2782623.27
Maltol	C6 H6 O3	Full match	Full match	Partial match	Full match	-	126.03195	2.799	2599740.77	26	12	0	89.2	2599740.77
PEG n11	C22 H46 O12	Not the top hit	Full match	No results	Full match	-	502.29909	4.284	2098519.253	0	2	0	88.5	2098519.25
Ginsenoside Rg3	C42 H72 O13	No match	Invalid mass	No match	No results	-	766.48533	5.588	1792976.447	1	4	0	83.2	1792976.45
Glycitin	C22 H22 O10	Not the top hit	Full match	Partial match	Full match	-	446.12103	4.439	1783088.822	11	2	0	86.7	1783088.82
L-Glutamic acid	C5 H9 N O4	Full match	Full match	Full match	Full match	-	147.05307	0.852	1748442.833	31	5	0	82.7	1748442.83
Bis(2-ethylhexyl) phth	C24 H38 O4	Not the top hit	Full match	Full match	Full match	-	390.2762	11.155	1545042.007	26	10	0	94.2	1545042.01
7,8-Dihydroxy-4-meth	C10 H8 O4	Full match	Full match	Not the top hit	Full match	-	192.04254	3.746	1252325.919	38	8	0	88.1	1252325.92
N,N'-Dicyclohexylurea	C13 H24 N2 O	Full match	Full match	Full match	Full match	-	224.18852	6.584	1171308.019	6	1	0	91.5	1171308.02
PEG n5	C10 H22 O6	Full match	Full match	Full match	Full match	-	238.14166	2.895	1165243.832	1	4	0	86.4	1165243.83
9-Oxo-10(E),12(E)-oc	C18 H30 O3	Full match	Full match	Not the top hit	Full match	-	294.21935	7.232	1003683.429	24	2	0	91.1	1003683.43
Naringenin	C15 H12 O5	Full match	Full match	Full match	Full match	-	272.06832	4.445	948756.3665	46	10	0	87.1	948756.367
Glucose 1-phosphate	C6 H13 O9 P	Full match	Full match	Partial match	Full match	-	260.02962	0.901	911408.6067	39	2	0	81	911408.607
Stearamide	C18 H37 N O	Full match	Full match	Full match	Full match	-	283.28703	10.658	885834.1188	4	2	0	92.1	885834.119
Guanine	C5 H5 N5 O	Full match	Full match	Partial match	Full match	-	151.04936	0.876	840032.1577	20	1	0	88.9	840032.158
Leucylproline	C11 H20 N2 O3	Full match	Full match	Partial match	Full match	-	228.1476	2.987	804307.6478	6	4	0	81.6	804307.648
PEG n13	C26 H54 O14	Not the top hit	Full match	No results	Full match	-	590.35113	4.469	759721.2017	0	1	0	87.3	759721.202
Uracil	C4 H4 N2 O2	Full match	Full match	Full match	Full match	-	112.02769	1.094	672279.754	28	3	0	83.4	672279.754
Monobutyl phthalate	C12 H14 O4	Full match	Full match	Partial match	Full match	-	222.0889	6.327	662943.6763	45	4	0	82.9	662943.676
L-Histidine	C6 H9 N3 O2	Full match	Full match	Full match	Full match	-	155.06949	0.833	659854.4891	18	2	0	88	659854.489
2-Hydroxycinnamic ac	C9 H8 O3	Full match	Full match	Partial match	Full match	-	164.04749	3.412	612912.9287	41	6	0	86.3	612912.929
Cyclo(leucylprolyl)	C11 H18 N2 O2	Full match	Full match	Partial match	No results	-	210.13686	4.27	571451.973	8	2	0	83.6	571451.973
Docosanamide	C22 H45 N O	Full match	Full match	No results	Full match	-	339.34957	13.101	446630.3886	0	1	0	88	446630.389
Diphenylamine	C12 H11 N	Full match	Full match	Full match	Full match	-	169.08913	7.451	430857.6066	15	2	0	84.3	430857.607
9S,13R-12-Oxophytod	C18 H28 O3	Full match	Full match	Partial match	Full match	-	292.20339	6.857	417031.1489	16	4	0	88.3	417031.149
Kojic acid	C6 H6 O4	Full match	Full match	Full match	Full match	-	142.02675	2.845	386314.3502	33	4	0	85	386314.35
Oleamide	C18 H35 N O	Full match	Full match	Full match	Full match	-	281.27159	9.863	367757.8594	4	1	0	92.3	367757.859
PEG n14	C28 H58 O15	Not the top hit	Full match	No results	Full match	-	634.37725	4.541	330815.8429	0	1	0	80.1	330815.843
Genistin	C21 H20 O10	Not the top hit	Full match	Not the top hit	Full match	-	432.10561	4.612	326649.1507	34	5	0	90.9	326649.151

(b)

Figure 5: Detection of CSD by high-resolution FTMS analysis. Illustration of part of a summary of the various abundant constituents detected and identified in CSD by channel of (a) methanol extraction and (b) pure water extraction.

xanthohumol, 7,8-dihydroxy-4-methylcoumarin, and naringenin. Meanwhile, quantitative monitoring of part of the components was illustrated in Figures 6 and 7. Simultaneously, the active ingredients by pure water extraction were as follows: oxymatrine, isoliquiritigenin, DL-stachydrine, cytisine, (+)-maackiain, 18-β-glycyrrhetinic acid, ginsenoside Rg3, 7,8-dihydroxy-4-methylcoumarin, and naringenin. Quantitative monitoring of part of the components was delineated in Figure 8.

4. Discussion

UCRCC is a malignant colonic disease and a multistep process with high mortality for which the accurate pathogenesis is inconclusive and well-appreciated effective therapy is limited. Recent advances have subscribed to the belief that continual inflammatory excitation structures a favourable background for UCRCC formation, providing proof that pivotal inflammatory mediators encompassing IL-6, TNF-α, NF-κB, and IL-17 (also called IL-17A) coupled with Th17 cells are enriched in UC and colorectal cancer [8, 30–34]. Given its remarkable therapeutic capacity of CSD in UC [19, 20], the concept has fueled our hypothesis that CSD may mitigate the progression of UCRCC to a certain degree. Delightedly, in our study, CSD demonstrates an inhibitory effect on the release of these inflammation-related cytokines and secretion of Th17 cells coinciding with reduced occurrence of polyp/tumor and preferable well-being. Thereupon, the outcomes may help to develop a mind map for the investigation of mechanism and therapy with respect to UCRCC.

Apoptosis conducted in the intrinsic pathway, mainly by the mitochondrial apoptosis-induced channel, is an essential practice of programmed cell death characterized by cellular morphological changes and death [35, 36]. Bcl-2 is localized to the outer membrane of mitochondria, where it exerts a significant role in promoting cellular survival and opposing the actions of pro-apoptotic proteins such as mitochondria-cleaved caspase-3 and caspase-9. Mitophagy is the selective degradation of malfunctioning or damaged mitochondria

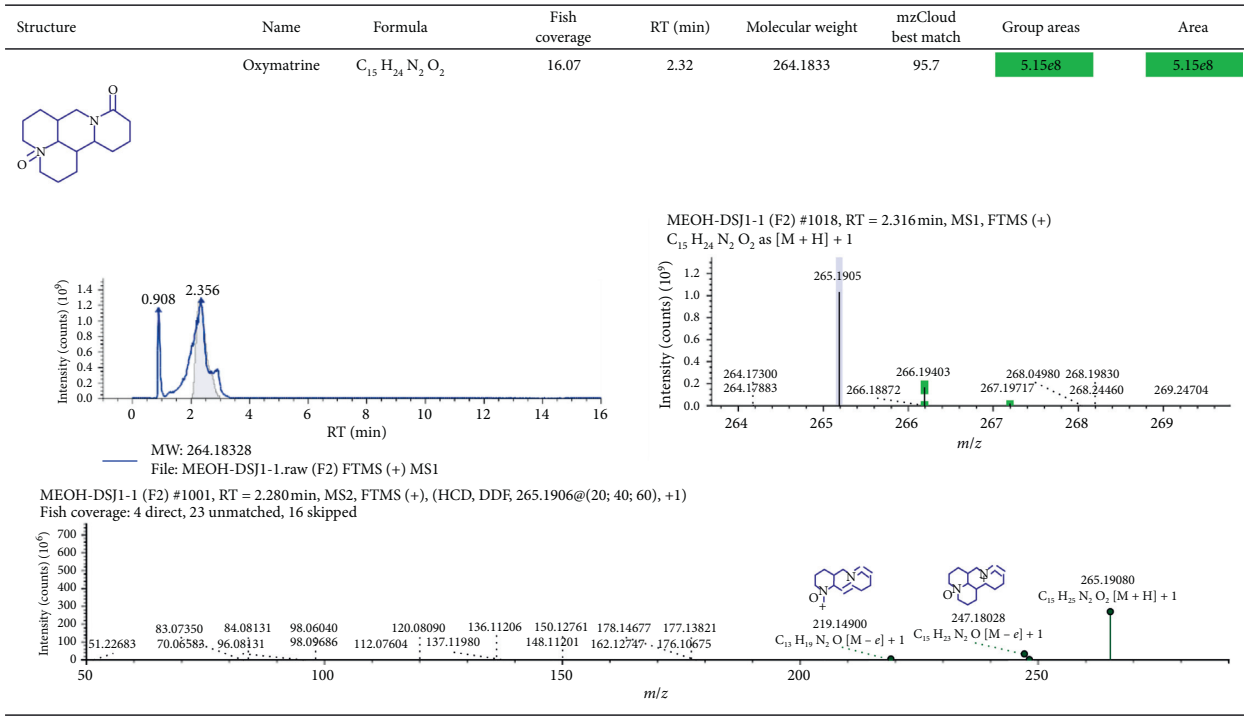

(a)

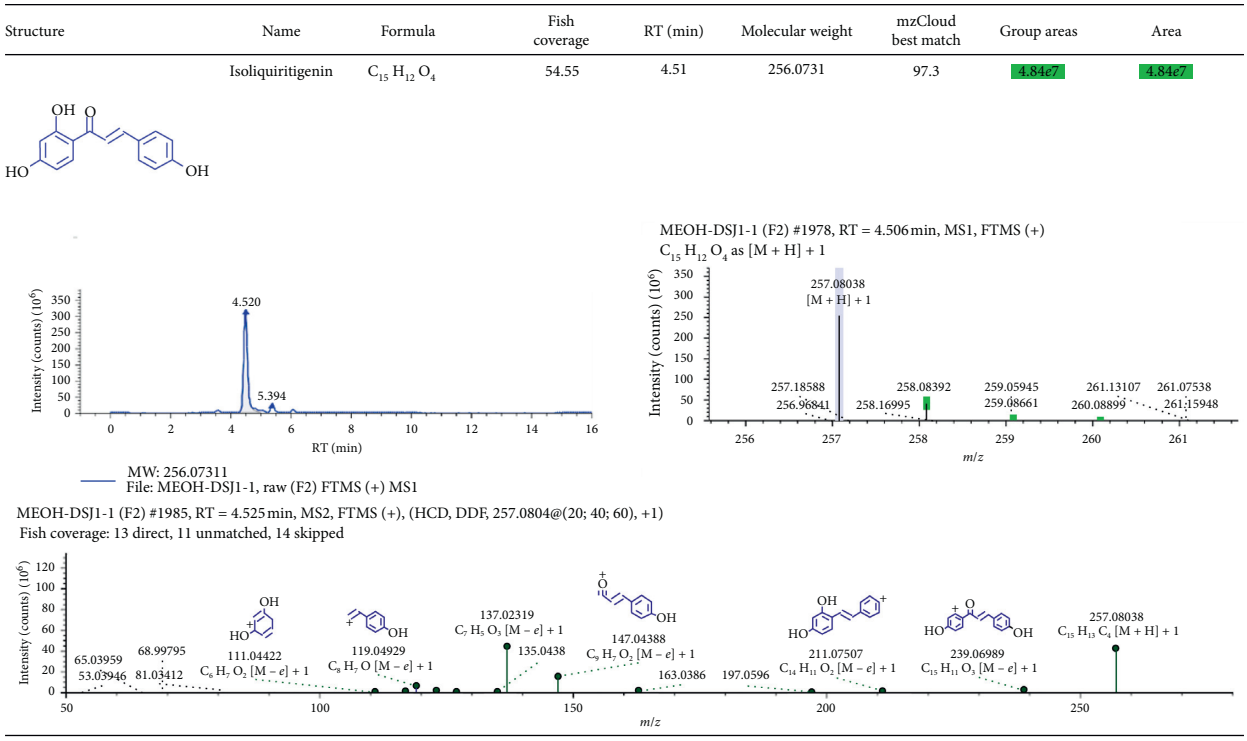

(b)

Figure 6: Positive-ion mode FTMS spectrum of the partial active ingredients from CSD extraction via methanol extraction. The active ingredients listed were oxymatrine (a) and isoliquiritigenin (b).

via autophagy to retain the mitochondrial quality, thus making cells adapted to various types of stress. Accumulating evidence has delineated a fundamental role of mitochondrial energy production and apoptotic mechanism in the tumor initiation [12, 16, 37]. The lipid composition of mitochondrial membrane has been reckoned capable of regulating mitochondrial membrane permeability and thence, cell death [11, 12, 38]. Considering the multifaceted

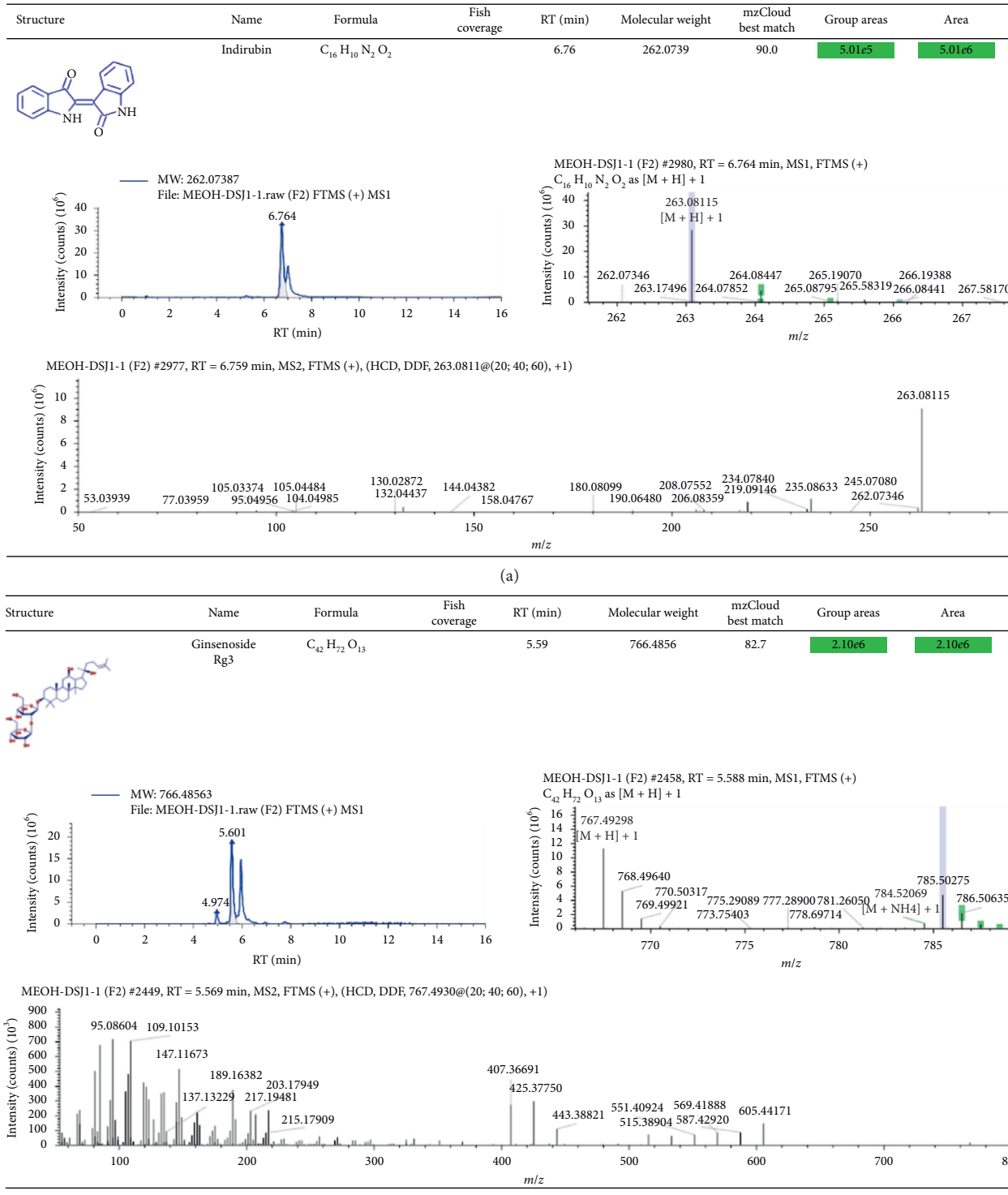

Figure 7: Positive-ion mode FTMS spectrum of the partial active ingredients from CSD extraction via methanol extraction. The active ingredients listed were indirubin (a) and ginsenoside Rg3 (b).

Structure	Name	Formula	Fish coverage	RT (min)	Molecular weight	mzCloud best match	Group areas	Area
	Oxymatrine	$C_{15}H_{24}N_2O_2$	14.55	2.36	264.1830	95.7	5.79e8	5.79e8

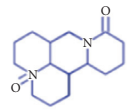

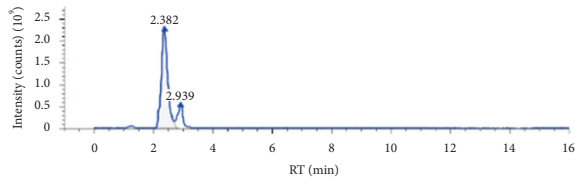

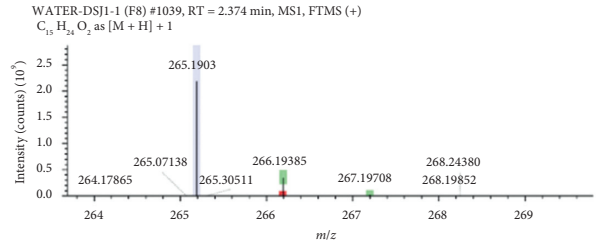

MW: 264.18303
File: WATER-DSJ1-1.raw (F8) FTMS (+) MS1

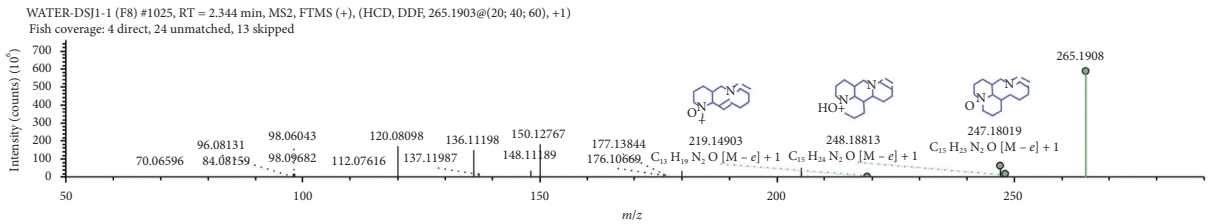

(a)

Structure	Name	Formula	Fish coverage	RT (min)	Molecular weight	mzCloud best match	Group areas	Area
	Isoliquiritigenin	$C_{15}H_{12}O_4$	45.10	4.51	256.0732	97.5	4.31e7	4.31e7

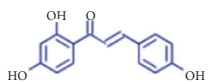

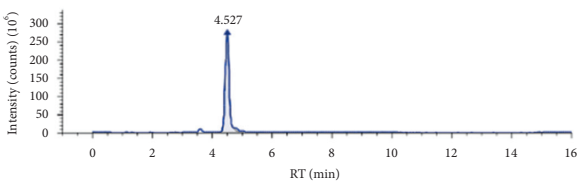

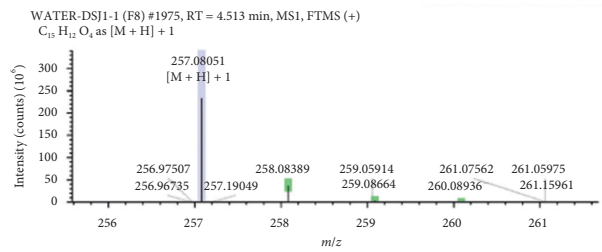

MW: 256.07320
File: WATER-DSJ1-1.raw (F8) FTMS (+) MS1

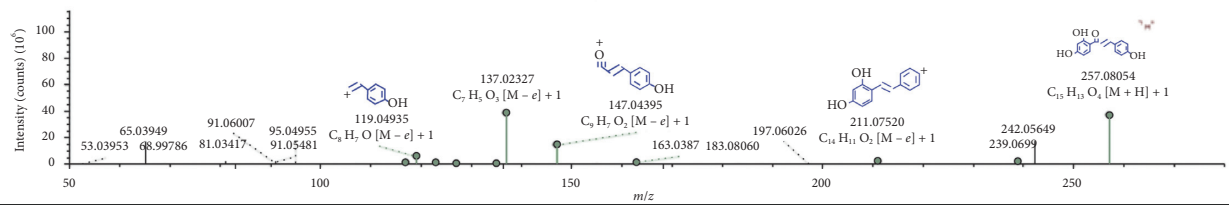

(b)

Figure 8: Continued.

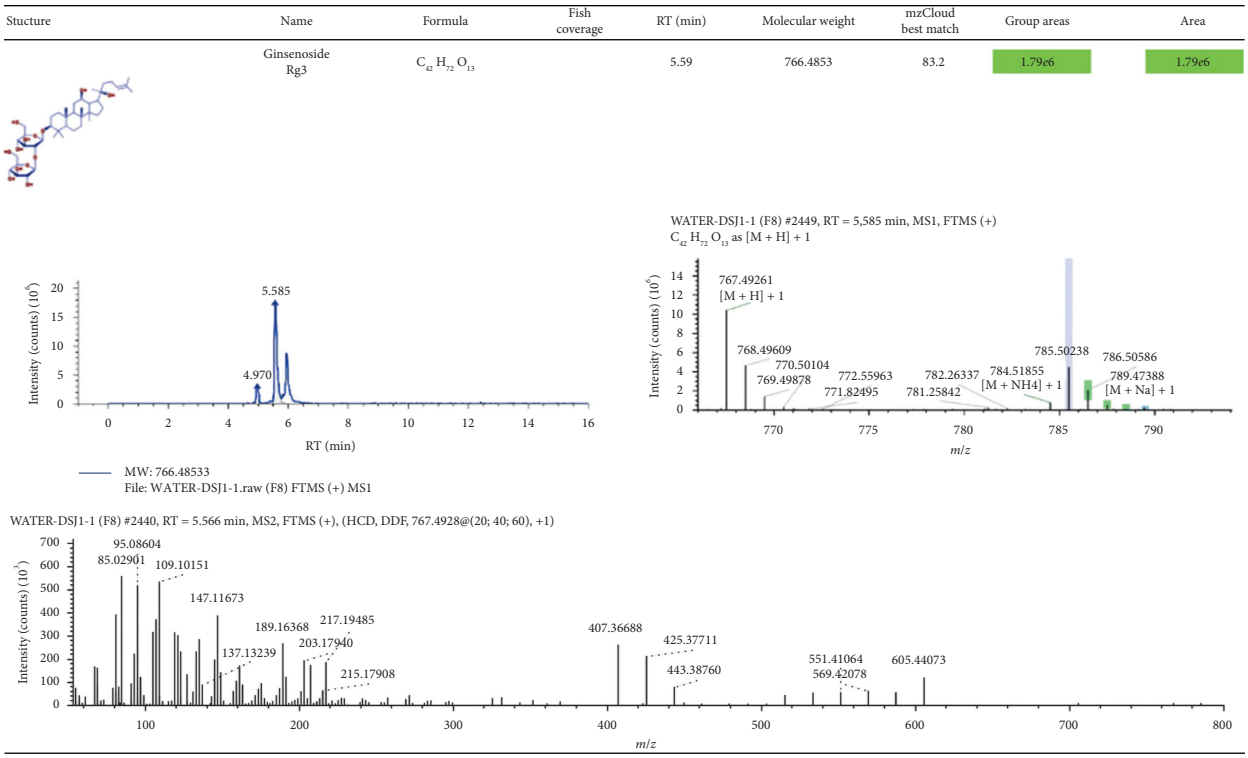

(c)

Figure 8: Positive-ion mode FTMS spectrum of the partial active ingredients from CSD extraction via pure water extraction. The active ingredients listed were oxymatrine (a), isoliquiritigenin (b), and ginsenoside Rg3 (c).

roles of mitochondria and intricate functions of mitophagy in tumorigenesis, care is exercised in the present study to decipher the role of the network comprising apoptosis, mitophagy, and inflammation responses in UCRCC and then to highlight innovative curative perception about UCRCC in support of the possibility that CSD can fine-tune the network.

Ultimately, our result that mitophagy and inflammation are positively joined to tumor progression in contrary to the fashion of apoptosis and CSD capsizes the trend remarkably may develop a new roadmap for the development of anti-tumor drugs for UCRCC.

Data Availability

The data used to support the findings of this study are available from the corresponding author upon request.

Conflicts of Interest

The authors declare that they have no conflicts of interest regarding the publication of this paper.

Authors' Contributions

Shuangjiao Deng, Qing Tang, and Xueyun Duan contributed equally to this work.

Acknowledgments

This work was supported by the National Natural Science Foundation of China (Nos. 81503433 and 81573784).

References

[1] J. A. Eaden, K. R. Abrams, and J. F. Mayberry, "The risk of colorectal cancer in ulcerative colitis: a meta-analysis," *Gut*, vol. 48, no. 4, pp. 526–535, 2001.

[2] M. Fumery, P. S. Dulai, S. Gupta et al., "Incidence, risk factors, and outcomes of colorectal cancer in patients with ulcerative colitis with low-grade dysplasia: a systematic review and meta-analysis," *Clinical Gastroenterology and Hepatology*, vol. 15, no. 5, pp. 665–674 e5, 2017.

[3] T. Jess, C. Rungoe, and L. Peyrin–Biroulet, "Risk of colorectal cancer in patients with ulcerative colitis: a meta-analysis of population-based cohort studies," *Clinical Gastroenterology and Hepatology*, vol. 10, no. 6, pp. 639–645, 2012.

[4] S. Grivennikov, E. Karin, J. Terzic et al., "IL-6 and Stat3 are required for survival of intestinal epithelial cells and development of colitis-associated cancer," *Cancer Cell*, vol. 15, no. 2, pp. 103–113, 2009.

[5] Y. S. Hyun, D. S. Han, A. R. Lee, C. S. Eun, J. Youn, and H.-Y. Kim, "Role of IL-17A in the development of colitis-associated cancer," *Carcinogenesis*, vol. 33, no. 4, pp. 931–936, 2012.

[6] M. Kathania, P. Khare, M. Zeng et al., "Itch inhibits IL-17-mediated colon inflammation and tumorigenesis by ROR-γt ubiquitination," *Nature Immunology*, vol. 17, no. 8, pp. 997–1004, 2016.

[7] N. Martin-Orozco, P. Muranski, Y. Chung et al., "T helper 17 cells promote cytotoxic T cell activation in tumor immunity," *Immunity*, vol. 31, no. 5, pp. 787–798, 2009.

[8] W. E. Naugler and M. Karin, "The wolf in sheep's clothing: the role of interleukin-6 in immunity, inflammation and cancer," *Trends in Molecular Medicine*, vol. 14, no. 3, pp. 109–119, 2008.

[9] M. F. Neurath and S. Finotto, "IL-6 signaling in autoimmunity, chronic inflammation and inflammation-associated cancer," *Cytokine & Growth Factor Reviews*, vol. 22, no. 2, pp. 83–89, 2011.

[10] N. Agnihotri, G. Sharma, I. Rani, B. A. Renuka, and A. Bhatnagar, "Fish oil prevents colon cancer by modulation of structure and function of mitochondria," *Biomedicine & Pharmacotherapy*, vol. 82, pp. 90–97, 2016.

[11] K. A. Boyle, J. van Wickle, R. B. Hill, A. Marchese, B. Kalyanaraman, and M. B. Dwinell, "Mitochondria-targeted drugs stimulate mitophagy and abrogate colon cancer cell proliferation," *Journal of Biological Chemistry*, vol. 293, no. 38, pp. 14891–14904, 2018.

[12] J. Y. Chang, H.-S. Yi, H.-W. Kim, and M. Shong, "Dysregulation of mitophagy in carcinogenesis and tumor progression," *Biochimica et Biophysica Acta (BBA)—Bioenergetics*, vol. 1858, no. 8, pp. 633–640, 2017.

[13] J. W. Choi, S. M. Son, I. Mook-Jung et al., "Mitochondrial abnormalities related to the dysfunction of circulating endothelial colony-forming cells in moyamoya disease," *Journal of Neurosurgery*, vol. 129, no. 5, pp. 1151–1159, 2018.

[14] C. Liu, J. Wang, Y. Yang et al., "Ginsenoside Rd ameliorates colitis by inducing p62-driven mitophagy-mediated NLRP3 inflammasome inactivation in mice," *Biochemical Pharmacology*, vol. 155, pp. 366–379, 2018.

[15] P.-P. Tan, B.-H. Zhou, W.-P. Zhao, L.-S. Jia, J. Liu, and H.-W. Wang, "Mitochondria-mediated pathway regulates C2C12 cell apoptosis induced by fluoride," *Biological Trace Element Research*, vol. 185, no. 2, pp. 440–447, 2018.

[16] S. Vyas, E. Zaganjor, and M. C. Haigis, "Mitochondria and cancer," *Cell*, vol. 166, no. 3, pp. 555–566, 2016.

[17] M. Zhu, Y. Tian, H. Zhang et al., "Methylphenidate ameliorates hypoxia-induced mitochondrial damage in human neuroblastoma SH-SY5Y cells through inhibition of oxidative stress," *Life Sciences*, vol. 197, pp. 40–45, 2018.

[18] H. Fan, X.-X. Liu, L.-J. Zhang et al., "Intervention effects of QRZSLXF, a Chinese medicinal herb recipe, on the DOR-β-arrestin1-Bcl2 signal transduction pathway in a rat model of ulcerative colitis," *Journal of Ethnopharmacology*, vol. 154, no. 1, pp. 88–97, 2014.

[19] H. Fan, J. Zhao, L. Shen et al., "Effect of compound sophorae flavescentis jiechangrong capsule on expression of NF-κB p65 and STAT6 in the intestinal mucosa of patients with ulcerative colitis," *Frontiers of Medicine in China*, vol. 3, no. 4, pp. 480–484, 2009.

[20] M. Xu, X.-Y. Duan, Q.-Y. Chen et al., "Effect of compound sophorae decoction on dextran sodium sulfate (DSS)-induced colitis in mice by regulating Th17/Treg cell balance," *Biomedicine & Pharmacotherapy*, vol. 109, pp. 2396–2408, 2019.

[21] Y. Gao, L.-F. Yao, Y. Zhao et al., "The Chinese herbal medicine formula mKG suppresses pulmonary fibrosis of mice induced by bleomycin," *International Journal of Molecular Sciences*, vol. 17, no. 2, p. 238, 2016.

[22] L. Gao, K.-X. Wang, Y.-Z. Zhou, J.-S. Fang, X.-M. Qin, and G.-H. Du, "Uncovering the anticancer mechanism of Compound Kushen Injection against HCC by integrating quantitative analysis, network analysis and experimental validation," *Scientific Reports*, vol. 8, no. 1, p. 624, 2018.

[23] X. He, J. Fang, L. Huang, J. Wang, and X. Huang, "Sophora flavescens Ait.: traditional usage, phytochemistry and pharmacology of an important traditional Chinese medicine," *Journal of Ethnopharmacology*, vol. 172, pp. 10–29, 2015.

[24] X.-Q. Wang, J. Liu, H.-S. Lin, and W. Hou, "A multicenter randomized controlled open-label trial to assess the efficacy of compound kushen injection in combination with single-agent chemotherapy in treatment of elderly patients with advanced non-small cell lung cancer: study protocol for a randomized controlled trial," *Trials*, vol. 17, no. 1, p. 124, 2016.

[25] B. Yanju, L. Yang, B. Hua et al., "A systematic review and meta-analysis on the use of traditional Chinese medicine compound kushen injection for bone cancer pain," *Supportive Care in Cancer*, vol. 22, no. 3, pp. 825–836, 2014.

[26] M. Yu, H.-M. Jia, F.-X. Cui et al., "The effect of Chinese herbal medicine formula mKG on allergic asthma by regulating lung and plasma metabolic alternations," *International Journal of Molecular Sciences*, vol. 18, no. 3, p. 602, 2017.

[27] C. Neufert, C. Becker, and M. F. Neurath, "An inducible mouse model of colon carcinogenesis for the analysis of sporadic and inflammation-driven tumor progression," *Nature Protocols*, vol. 2, no. 8, pp. 1998–2004, 2007.

[28] S. Deng, H. Wang, H. Fan et al., "Over-expressed miRNA-200b ameliorates ulcerative colitis-related colorectal cancer in mice through orchestrating epithelial-mesenchymal transition and inflammatory responses by channel of AKT2," *International Immunopharmacology*, vol. 61, pp. 346–354, 2018.

[29] E. Giner, M. C. Recio, J. L. Ríos, J. M. Cerdá-Nicolás, and R. M. Giner, "Chemopreventive effect of oleuropein in colitis-associated colorectal cancer in c57bl/6 mice," *Molecular Nutrition & Food Research*, vol. 60, no. 2, pp. 242–255, 2016.

[30] V. De Simone, F. Pallone, G. Monteleone, and C. Stolfi, "Role of TH17 cytokines in the control of colorectal cancer," *Oncoimmunology*, vol. 2, no. 12, Article ID e26617, 2013.

[31] J. C. Mazzei, H. Zhou, B. P. Brayfield, R. Hontecillas, J. Bassaganya-Riera, and E. M. Schmelz, "Suppression of intestinal inflammation and inflammation-driven colon cancer in mice by dietary sphingomyelin: importance of peroxisome proliferator-activated receptor γ expression," *The Journal of Nutritional Biochemistry*, vol. 22, no. 12, pp. 1160–1171, 2011.

[32] S. Punt, J. M. Langenhoff, H. Putter, G. J. Fleuren, A. Gorter, and E. S. Jordanova, "The correlations between IL-17 vs. Th17 cells and cancer patient survival: a systematic review," *Oncoimmunology*, vol. 4, no. 2, Article ID e984547, 2015.

[33] X. Wang, L. Yang, F. Huang et al., "Inflammatory cytokines IL-17 and TNF-α up-regulate PD-L1 expression in human prostate and colon cancer cells," *Immunology Letters*, vol. 184, pp. 7–14, 2017.

[34] C. M. Wilke, I. Kryczek, S. Wei et al., "Th17 cells in cancer: help or hindrance?," *Carcinogenesis*, vol. 32, no. 5, pp. 643–649, 2011.

[35] B. Guo, M. Yang, D. Liang, L. Yang, J. Cao, and L. Zhang, "Cell apoptosis induced by zinc deficiency in osteoblastic MC3T3-E1 cells via a mitochondrial-mediated pathway," *Molecular and Cellular Biochemistry*, vol. 361, no. 1-2, pp. 209–216, 2012.

[36] S. Mukhopadhyay, P. K. Panda, N. Sinha, D. N. Das, and S. K. Bhutia, "Autophagy and apoptosis: where do they meet?," *Apoptosis*, vol. 19, no. 4, pp. 555–566, 2014.

[37] F. Jiang, J. Y. Zhou, D. Zhang, M. H. Liu, and Y. G. Chen, "Artesunate induces apoptosis and autophagy in HCT116 colon cancer cells, and autophagy inhibition enhances the artesunate-induced apoptosis," *International Journal of Molecular Medicine*, vol. 42, no. 3, pp. 1295–1304, 2018.

[38] M. van der Ende, S. Grefte, R. Plas et al., "Mitochondrial dynamics in cancer-induced cachexia," *Biochimica et Biophysica Acta (BBA)—Reviews on Cancer*, vol. 1870, no. 2, pp. 137–150, 2018.